

**Low thermal conductivity of graphyne nanotubes from molecular dynamics study**Ming Hu,<sup>1,2,\*</sup> Yuhang Jing,<sup>3</sup> and Xiaoliang Zhang<sup>1</sup><sup>1</sup>*Institute of Mineral Engineering, Division of Materials Science and Engineering, Faculty of Georesources and Materials Engineering, Rheinisch-Westfaelische Technische Hochschule (RWTH Aachen University), 52064 Aachen, Germany*<sup>2</sup>*Aachen Institute for Advanced Study in Computational Engineering Science (AICES), RWTH Aachen University, 52062 Aachen, Germany*<sup>3</sup>*Department of Astronautical Science and Mechanics, Harbin Institute of Technology, Harbin 150001, China*

(Received 17 November 2014; revised manuscript received 3 February 2015; published 9 April 2015)

It is well known that carbon nanotubes (CNTs) possess ultrahigh thermal conductivity that is comparable to bulk diamond. However, no research has studied the possible low thermal conductivity of different CNTs so far. By performing nonequilibrium molecular dynamic simulations, we reveal that the perfect graphyne nanotube (GNT) exhibits an unprecedentedly low thermal conductivity (below 10 W/mK at room temperature), which is generally two orders of magnitude lower than that of ordinary CNTs and even lower than the values reported for defected, doped, and chemically functionalized CNTs. By performing phonon polarization and spectral energy density analysis, we observe that the ultralow thermal conductivity stems from the unique atomic structure of the GNT, consisting of the weak acetylenic linkage ( $sp$  C-C bonds) and the strong hexagonal ring ( $sp^2$  C-C bonds), which results in a large vibrational mismatch between these two components, and thus induces significantly inefficient heat transfer. Moreover, the thermal transport in GNT with a large number of acetylenic linkages is dominated by the low frequency longitudinal modes in the linkage. Such strong confinement of the low frequency thermal energy results in the extremely low thermal conductivity due to the flattened phonon dispersion curves (low phonon group velocities). The exploration of the abnormal thermal transport of GNTs paves the way for design and application of the relevant devices that could benefit from the ultralow thermal conductivity, such as thermoelectrics for energy conversion.

DOI: [10.1103/PhysRevB.91.155408](https://doi.org/10.1103/PhysRevB.91.155408)

PACS number(s): 65.80.-g, 63.22.-m, 63.22.Kn

**I. INTRODUCTION**

Carbon nanotubes (CNTs) [1,2], with extraordinary mechanical, physical, and chemical properties and the wide prospects for their technological use, have generated an enormous amount of research interest and activities since their discovery. Exciting phenomena have been observed, including field emission [3], quantum conductance [4], superconductivity [5], and extremely high thermal conductivity [6,7], as well as proposals of various CNT-based devices [8,9]. Depending upon structure, CNTs are either metallic or semiconducting, which is a feature that has been intensively investigated and exploited in prototype devices. While previous papers have focused on graphitic nanotubes, recent research indicates that other types of pure CNTs are feasible using different accessible hybridization states of carbon. One possibility that has been overlooked in the literature is to use graphyne sheets as the structural motif for CNTs. Graphyne, consisting of planar molecular sheets containing  $sp$  and  $sp^2$  carbon atoms, is an allotropic form of carbon proposed by Baughman *et al.* [10] in 1987, and has recently become the focus of new investigations [11–15]. Graphyne nanotube (GNT) is a special type of CNT with the lowest energy, which can be formed by rolling up the graphyne sheets to generate quite different seamless cylinders. Experimental success has been achieved in the synthesis of graphdiyne nanotube arrays through an anodic aluminum oxide template [16], which shows the graphdiyne nanotube arrays possess high-performance field emission properties. Although the wall thickness of the graphdiyne nanotube obtained is

15 nm, which is far from the single-walled carbon nanotube, we anticipate that the synthesis of single-walled graphyne-based nanotubes may be achieved in the near future. The presence of acetylenic groups in these structures introduces a rich variety of optical and electronic properties that are quite different from those of ordinary CNTs [17–26]. For example,  $\alpha$ -GNTs present electronic properties similar to the usual CNTs, while armchair  $\beta$ -GNTs are metallic, and zigzag ones present either metallic or semiconducting behavior, depending on a fractional rule for the tube index [21]. Wang *et al.* [25] show that by decorating GNTs with calcium, the storage capacity of  $H_2$  can reach 7.44 wt%, suggesting that Ca decorated GNTs can be used as a promising hydrogen storage system. By using a nonequilibrium Green's function method, Wang and Lu [26] found that the maximum value of the figure of merit ( $ZT$ ) can reach as high as 0.83 for the (3, 0) GNT at room temperature, which shows the GNT is very promising for thermoelectrics.

Although in recent years a considerable amount of interest has been dedicated to the investigation of electronic structure and electronic transport properties of GNTs, to the best of our knowledge, the thermal transport (mainly phonons) property of such an allotropic CNT system of interest has not been investigated. As GNTs would be used as electronics in the near future, people are also very interested in their thermal transport properties, since the thermal conductivity is one of the crucial physical parameters in device design and function. It is well known that the stiff  $sp^2$  C-C bonds in the atomically perfect nanotube cylinders render the CNT with an extremely high thermal conductivity, which is measured to be  $\sim 3400$  W/mK for a single-walled CNT, with a length of  $2.6 \mu\text{m}$  at room temperature [27]. Theoretical study also reveals that the thermal conductivity of thin CNTs increase with the decreasing diameters [28]. Therefore, one might intuitively expect that

\*Author to whom correspondence should be addressed: hum@ghi.rwth-aachen.de

the GNTs should also intrinsically have a high thermal conductivity because of its similar cylinderlike quasi-one-dimensional (1D) structure as CNTs and the extremely small diameter that GNTs can form. However, this might not be true due to the unique bonding topography of GNTs consisting of the combined  $sp$  and  $sp^2$  carbon bonds with quite different vibrational properties.

In this paper, we investigate the phonon transport of GNTs using nonequilibrium molecular dynamics (NEMD) simulations. The effects of the number of acetylenic linkages, length, and nanotube diameter on the thermal conductivity are explicitly considered. The paper is organized as follows: In Sec. II, we give our model system and computational details. In Sec. III, we report the lattice thermal conductivity of GNTs as a function of the number of acetylenic linkages. The extremely low thermal conductivity found for GNTs is even one order of magnitude lower than that for the small diameter (2, 1) CNT reported recently [29]. The salient feature of the unprecedentedly low thermal conductivity of GNTs is also identified, comparing it with ordinary CNTs. The governing mechanism is explained in terms of the vibrational mismatch between the weak acetylenic carbon ( $sp$ ) and the strong graphene hexagonal carbon ( $sp^2$ ). The unusual phonon transport mechanism is then consolidated by quantitatively determining the relative contributions from different regions of the graphyne structure to the overall lattice thermal transport and comparing the phonon lifetime between different GNTs. In Sec. IV, we studied the length and diameter dependence of the thermal conductivity of GNTs. In Sec. V, we summarize and conclude our results.

## II. MODEL STRUCTURE AND SIMULATION METHODOLOGY

Our model systems consist of graphyne  $n$  nanotubes in both the armchair and zigzag directions, where “ $n$ ” is defined as the number of acetylenic linkages (corresponding to  $2 \times n$  carbon atoms) between the nearest neighboring carbon hexagons. The acetylenic linkages are initially constructed based on the *ab initio* calculations in a previous paper [30], and C-C bonds alternate between triple and single bonds. The C-C bond lengths are different for various types of bonding. Molecular dynamics (MD) cannot make the difference between the two types of bonding, and we can only judge the bonding type according to the initial structures we constructed. However, all model structures were constructed based on the optimized graphyne sheets using *ab initio* calculations in our previous paper. A representative GNT is shown in Fig. 1. In all MD simulations performed herein, the adaptive intermolecular reactive empirical bond order (AIREBO) potential derived from the second-generation Brenner potential [31] is used to describe the interactions between carbon atoms. The AIREBO potential is widely used in MD simulations of carbon systems and provides accurate representations of the lattice dynamics and phonon thermal transport in carbon related systems (see details in Sec. III A) [32–37].

All MD simulations are performed using the Large Scale Atomic/Molecular Massively Parallel Simulator (LAMMPS) package [38]. The velocity Verlet algorithm is employed to integrate the equations of motion with a time step of

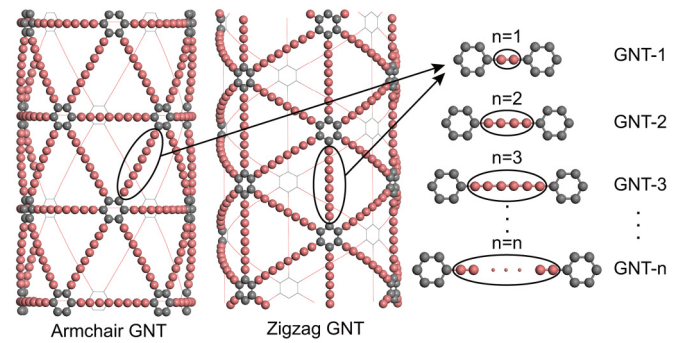


FIG. 1. (Color online) A representative armchair and zigzag graphyne  $n$  nanotube structure with the definition of  $n$ .

0.55 fs. All systems were equilibrated at a constant pressure of 1 atm along the tube axis and a temperature of 300 K using the isothermal-isobaric ( $NPT$ ; constant number of particles, pressure, and temperature) ensemble for 500 ps. The temperature is controlled by employing the Nosé-Hoover thermostat [39,40]. After the  $NPT$  simulation, we continued to relax the system with a microcanonical ( $NVE$ ; constant volume and no thermostat) ensemble for 250 ps. During this stage, we monitored the total energy and temperature of the entire system. We found that the total energy conserved very well, and the temperature remained constant with small fluctuations around 300 K, which meant that the system had reached the equilibrium state.

Following equilibration, the thermal conductivity of the GNTs is computed using NEMD. The constant heat flux is imposed by the Müller-Plathe method [41]. The outmost few unit cells of the GNT on both ends ( $\sim 0.3$  nm long) are fixed, and the nearby slices with a length  $\sim 4$  nm are defined as “hot slab” and “cold slab,” respectively. The nonperiodic boundary condition is used in the longitudinal direction. The coldest atoms in the hot slab and the hottest atoms in the cold slab are selected, and their kinetic energies are exchanged every 800 to 20 000 time steps, depending on the thermal conductivity of the structure, to maintain a temperature difference between the hot and cold slab to be around 30 K (10% of system temperature). This operation will induce a constant heat flux in the system and also a temperature gradient along the heat flux direction after running some time. The thermal conductivity is finally calculated by Fourier’s law

$$\kappa = -\frac{J_L}{\partial T/\partial y}, \quad (1)$$

where  $J_L$  is the averaged heat flux along the tube axis ( $y$ , longitudinal direction) and  $\partial T/\partial y$  is the temperature gradient determined from the linear fitting to the temperature profile. For the cross-sectional area, we used the common formula  $A = \pi dh$ , where  $d$  and  $h$  are the diameter and thickness (0.335 nm) of the GNTs, respectively. Note that when we output the temperature profile, we divided the system into slices, each containing at least 400 atoms to ensure a small fluctuation during averaging. Each temperature profile is averaged over 250 ps. Once the steady state is reached, which typically takes  $\sim 4$  ns, depending on the system, we run at least an additional 15 ns to collect data to obtain the heat flux (by linear fitting

the accumulated exchange of heat with respect to time) and temperature gradient (by linear fitting the average temperature profile with respect to longitudinal position).

### III. PHONON TRANSPORT MECHANISM

#### A. Effect of the length of acetylenic linkages

We first study the dependence of the thermal conductivity of the GNT on the length of acetylenic linkages (number  $n$ ). The results are shown in Fig. 2. All GNTs are 500 nm long in the longitudinal direction, along which the heat flux is imposed, and around 3.4 nm in diameter. We assume the thickness of the GNTs to be 0.335 nm (the same as that of ordinary CNTs). It is well known that the thermal conductivity of nanostructures calculated by NEMD strongly depends on the simulation length, which will be investigated in detail later. From Fig. 2, we first notice that the thermal transport in the GNT is perfectly isotropic, i.e., the thermal conductivity of GNTs is independent of the longitudinal direction. A more salient feature in Fig. 2 is that the thermal conductivity of both armchair and zigzag GNTs is extremely low. The thermal conductivity value is generally two orders of magnitude lower than that of ordinary perfect CNTs, which range from several hundred to a few thousand watts per meter Kelvin [6,7,27], and is even lower than the values reported for defected, doped, and chemically functionalized CNTs [42–46]. The reduction is primarily due to the weak single C-C bonds in the acetylenic linkages and the large vibrational mismatch between the linkage and the ring, as we will reveal next. Moreover, for comparison, we also show the thermal conductivity of (2, 2) CNT (373.4 W/mK calculated separately) and (2, 1) CNT (80.45 W/mK taken from Ref. [29]) with a length of 100 nm. We see that the thermal conductivity of GNTs is significantly lower than that found for the ultrathin (2, 1) CNT [29]. For instance, the thermal conductivity of armchair and zigzag GNT-10 is as low as 7.04 and 8.24 W/mK, respectively, which is even one order of magnitude lower than that for (2, 1) CNT. This establishes a new low value for the thermal conductivity of the allotropic CNTs. The previously reported low thermal conductivity for (2, 1) CNT is believed to originate from the softening of acoustic phonon modes, leading to small group velocities and the great reduction in the phonon lifetimes [29]. As we will see later, the mechanism of the extremely low thermal conductivity of GNTs is fundamentally different.

The AIREBO potential underestimates the thermal conductivities in CNTs and graphene [47] because the AIREBO potential yields suppressed phonon dispersion relations resulting in underestimated group velocities as compared to the experimental values. However, the AIREBO potential explicitly considers  $\sigma$  and  $\pi$  interactions between carbon atoms and provides the improvements on the carbon nanostructure with mixed single, double, and triple C-C bonds. Our separate *ab initio* calculation shows that AIREBO potential can quantitatively reproduce different bonding lengths between triple and single bonds in the model structures we used in this paper. We also tried the optimized Tersoff potential [48], but it turns out that the optimized Tersoff potential, although it works very well with ordinary CNTs, cannot maintain the correct atomic structure for GNTs. Since this paper focuses more on

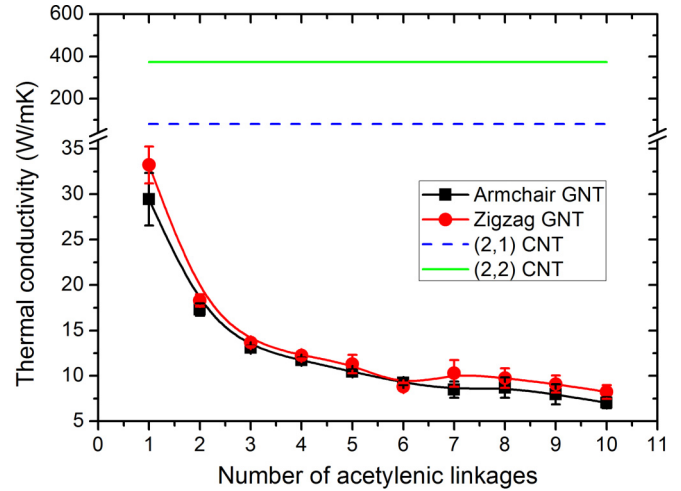


FIG. 2. (Color online) Dependence of thermal conductivity of armchair and zigzag GNTs on the number of acetylenic linkages. All GNTs are 500 nm long. The thermal conductivity of ordinary (2, 2) and (2, 1) CNTs is shown by a horizontal solid line (373.4 W/mK for 100 nm length) and dashed line (80.45 W/mK for 100 nm length, taken from Ref. [29]), respectively.

the relatively low thermal conductivity of GNTs as compared with ordinary CNTs, the AIREBO potential is the only suitable interatomic potential that we can use to reveal this phenomenon and the underlying mechanism. Certainly note that the thermal conductivity values reported for GNTs ( $\sim 7$ – $8$  W/mK) cannot be taken as quantitative. Moreover, the quantum effects that are neglected in the MD simulation can also influence the absolute values of thermal conductivity of carbon materials. Nevertheless, we expect that our finding of the relatively low thermal conductivity of GNTs will inspire others to use more accurate method to calculate the thermal conductivity, such as *ab initio* based anharmonic lattice dynamics simulation coupled with the Boltzmann transport equation.

Another notable feature in Fig. 2 is the monotonic dependence of thermal conductivity of GNTs on the number of acetylenic linkages. The thermal conductivity of GNTs decreases steeply with number of acetylenic linkages increasing ( $n \leq 5$ ). Then, the thermal conductivity decreases slightly when the number of acetylenic linkages increases further (for  $5 < n \leq 10$  considered here). At first glance, the trend is understandable: we know that the high thermal conductivity of ordinary CNTs relies on the perfect hexagonal lattice and strong  $sp^2$  C-C bonds. Inserting acetylenic linkages can deteriorate the stability of the original honeycomb structure, and the stiffness could be reduced further when increasing the acetylene linkages. Thus, the thermal conductivity of graphyne structures is anticipated to decrease with the increase of acetylenic linkages. The detailed mechanism is described below.

#### B. Vibrational density of states

To understand the mechanism of the low thermal conductivity of GNTs, we first calculated the normalized vibrational density of states (VDOS) via a Fourier transform of the atomic velocity autocorrelation function of carbon atoms on the

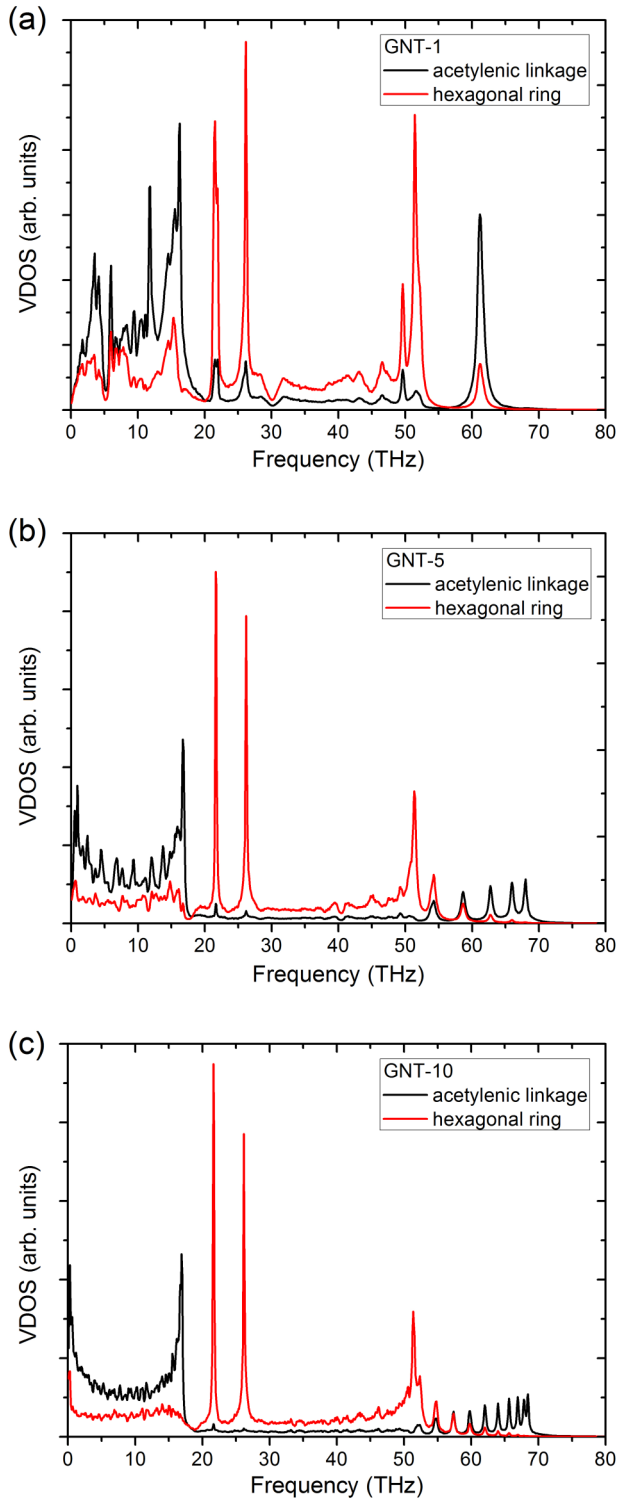


FIG. 3. (Color online) Comparison of phonon VDOS of carbon atoms in the acetylenic linkage and hexagonal ring for (a) GNT-1, (b) GNT-5, and (c) GNT-10. All GNTs are zigzag in longitudinal direction.

acetylenic linkages and hexagonal rings separately, as shown in Fig. 3. It can be seen that the phonons of carbon atoms on the acetylenic linkages are mainly concentrated in the low frequency range (0–15 THz), while the phonons of carbon atoms in the hexagonal rings are dominated by few high frequency

peaks in the range of 20–55 THz. As the number of acetylenic linkages increases, the number of peaks in the low frequency VDOS (acetylenic linkages) increases, and in the meantime, the VDOS in the high frequency range of 20–55 THz disappears. In contrast, the low frequency VDOS of hexagonal rings decreases largely and the high frequency VDOS is enhanced, especially for the frequency range of 20–55 THz. This results in a large reduction of the overlap area of VDOS between the acetylenic linkage and hexagonal ring atoms. In other words, as the number of acetylenic linkages increases, the vibrational mismatch between the linkage and ring becomes larger, or coupling becomes weaker, which leads to the significant reduction in thermal conductivity, as shown in Fig. 2.

We also analyzed the relative contribution of the acetylenic linkage and hexagonal ring atoms to the overall heat transport. This was realized by defining the “local” heat flux onto a single atom by determining the contribution of every atom to each term in the heat flux formula [49]

$$J_L(t) = \frac{1}{V} \left[ \sum_i v_{i,L} \varepsilon_i + \frac{1}{2} \sum_{i,j,i \neq j} r_{ij,L} (\vec{f}_{ij} \cdot \vec{v}_j) + \sum_{i,j,k} r_{ij,L} (\vec{f}_j(ijk) \cdot \vec{v}_j) \right], \quad (2)$$

where the subscript “ $L$ ” denotes a quantity in the longitudinal direction,  $v_i$  is the velocity of atom  $i$ ,  $\varepsilon_i$  the local site energy,  $r_{ij}$  the relative distance between atom  $i$  and  $j$ ,  $\vec{f}_{ij}$  the two-body force between atom  $i$  and  $j$ ,  $\vec{f}_j(ijk)$  the three-body interactions between atoms  $i$ ,  $j$ , and  $k$ , and  $V$  the control volume of the region selected to calculate the heat flux. In this calculation, a slice with a length of 100 nm in the middle of the structure along the axial direction (heat flux direction) is selected, and the heat flux on each selected atom is averaged over 11 ns. This method has been successfully used to analyze the heat conduction in other nanostructures in our previous papers [50,51]. Actually there are two “different” ways to examine the heat flux: the control volume method [Eq. (2)] and the interface method [the latter in Eq. (3)]. But these two methods have been proved to be equivalent recently [52]. In the control volume method, the heat flux is understood as the heat current carried by the whole ensemble (all the atoms) inside the control volume [that is also why the heat flux in Eq. (2) is finally divided by the volume], and in this way, one can define the heat flux contribution of a partial group of atoms to the overall value, while in the interface method, the heat flux is characterized by the “work” that is applied to the atoms on one side of the interface due to the atoms on the other side (the interface separates these two groups of atoms, and only the cross-interface interactions contribute to the heat flux). Therefore, for the control volume method, the cross section is not involved in the atomic heat flux calculation. In contrast, for the interface method, the cross section is involved, and for this method, the heat current through any cross section in the GNT is the same. Moreover, since we chose a significantly long length in the heat flux direction (100 nm) as the control volume, there is a large enough number of atoms in the control volume for sampling; thus, the atomic heat flux calculated by Eq. (2) is also independent of the choice of the length.

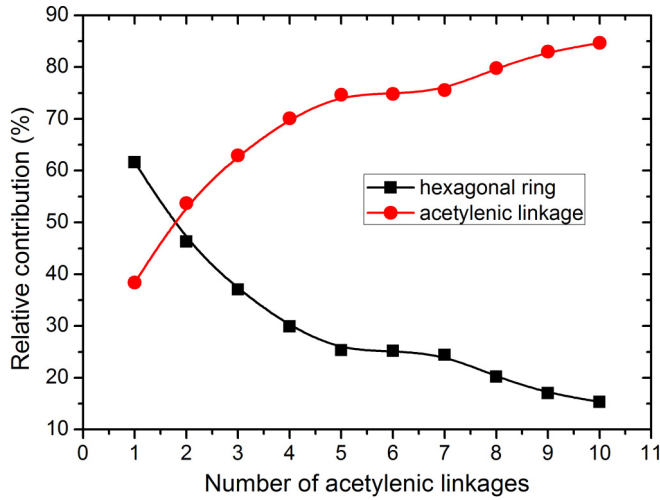


FIG. 4. (Color online) Relative contribution (percentage) of vibrations from the acetylenic linkage and hexagonal ring atoms to total heat flux of GNTs as a function of number of acetylenic linkages. All GNTs are zigzag in longitudinal direction and 500 nm long.

Figure 4 shows the relative contribution of the acetylenic linkage and hexagonal ring atoms to the total heat flux of GNTs as a function of the number of acetylenic linkages. It is clearly seen that when the number of acetylenic linkages is small, the overall thermal transport is dominated by the vibrations from hexagonal ring atoms. As the number of acetylenic linkages increases, this contribution gradually decreases, and at the same time, the contribution from the acetylenic linkages atoms increases, indicating that the heat flux is localized to the carbon atoms in the acetylenic linkages. Moreover, note that such a vibration of the acetylenic linkage atoms mainly comes from the low frequency in-plane phonons, as evidenced by VDOS, shown in Fig. 3. Due to the weak coupling between the acetylenic linkage and hexagonal ring atoms, the thermal energy transport between these two components is inefficient. The strong confinement of the thermal energy to the acetylenic linkages results in the extremely low thermal conductivity of GNTs.

### C. Phonon polarization analysis

The above lattice vibration mismatch can be further proved by performing phonon polarization analysis. To this end, we followed the method we proposed recently [53] to quantify the relative contributions of longitudinal and transverse modes to the overall phonon transport as

$$J_{\text{left} \rightarrow \text{right}, \alpha} = -\frac{1}{2A} \sum_{i \in \text{left}} \sum_{j \in \text{right}} F_{ij\alpha} (v_{i\alpha} + v_{j\alpha}), \quad (3)$$

where  $J_{\text{left} \rightarrow \text{right}, \alpha}$  is the heat flux across an imaginary interface (in the middle of the structure, by which the atoms on both sides are defined as “left” and “right” groups) contributed by the lattice vibrations in the  $\alpha$  direction,  $\alpha$  can be the longitudinal (y) and transverse (x and z),  $A$  is the cross-sectional area of GNTs,  $F_{ij\alpha}$  is the  $\alpha$  component of the force acting on atom  $i$  due to atom  $j$ ,  $v_{i\alpha}$  is the  $\alpha$  component of the velocity of atom  $i$ , and the two sums are taken over atoms  $i$  and  $j$

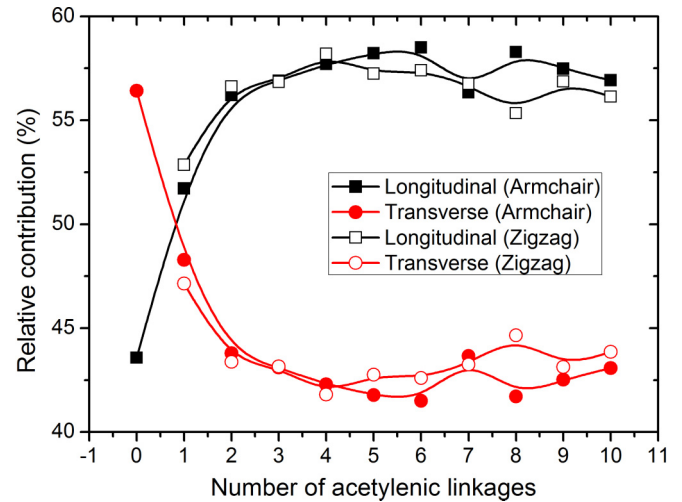


FIG. 5. (Color online) Relative contribution (percentage) to total heat flux of GNTs from lattice vibrations in longitudinal (y) and transverse (x and z) directions as a function of the number of acetylenic linkages. All GNTs are 500 nm long. Zero number of acetylenic linkages refers to ordinary (2, 2) CNT.

belonging to the group of left and right, respectively. The computational details can be found in Ref. [53]. This method has been successfully used for explaining the phonon transport mechanism in various nanostructures [34,54–56]. Moreover, it should be straightforward to decompose the heat current into radial and azimuthal contributions for GNTs, but in this paper, we are more concerned about the relative change of the longitudinal and transverse mode contribution with the number of acetylenic linkages. Therefore, we still decompose the heat current into regular coordinate directions, corresponding to longitudinal and transverse modes, not into radial and azimuthal directions.

Figure 5 shows the relative contribution to the total heat flux from the lattice vibrations in the longitudinal and transverse directions as a function of number of acetylenic linkages. When the number of acetylenic linkages is zero, it refers to ordinary (2, 2) CNT. As we can see for both ordinary CNTs and GNTs with small numbers of acetylenic linkages, the transverse vibrations contribute the most to the total heat flux. As the number of acetylenic linkages increases, the contribution to the total thermal transport from the transverse modes gradually decreases, and at the same time, the contribution from the longitudinal modes increases. For the number of acetylenic linkages larger than five, the contribution from longitudinal modes reaches a plateau. It is interesting to see that the converging point ( $n = 5$ ), where the relative contribution from longitudinal and transverse modes does not change anymore, is exactly the same position as found in Fig. 2, where the thermal conductivity of GNTs decreases at a much slower pace, with the number of acetylenic linkages increasing further. Combining Fig. 5 with Figs. 3 and 4, we confirm our previous statement that the extremely low thermal conductivity of GNTs for a large number of acetylenic linkages originates from the dominance of the heat conduction from the *low frequency longitudinal modes* in the acetylenic linkages.

#### D. Phonon spectral energy density analysis

To gain more insight into the mechanism for the effect of the number of acetylenic linkages on the thermal conductivity of GNTs, we calculated the frequency-dependent phonon lifetime by performing spectral energy density (SED) analysis. The phonon normal mode is obtained by [57]

$$\dot{Q}(\vec{k}, \nu, t) = \sum_{jl} \sqrt{\frac{m_j}{N}} \vec{v}_{jl}(t) \cdot \vec{e}_j^*(\vec{k}, \nu) \exp(-2\pi i \vec{k} \cdot \vec{r}_l). \quad (4)$$

Then, the SED is calculated by [58]

$$\Phi(\vec{k}, \nu, f) = \left| \int \dot{Q}(\vec{k}, \nu, t) \exp(-2\pi i f t) dt \right|^2, \quad (5)$$

and the phonon lifetime is obtained by fitting the Lorentzian function [59]. The frequency dependent phonon lifetime of GNTs with different numbers of acetylenic linkages are compared in Fig. 6. For GNT-1, the majority of the medium and high frequency phonons have a considerably large phonon lifetime, leading to significantly higher thermal conductivity than the other two cases. As the length of the acetylenic linkages increases (GNT-5 and GNT-10), the phonon lifetime in the medium and high frequency range significantly drops down, and at the same time, more phonons are populated in the low frequency range (lower than 1 THz). This result is consistent with Figs. 4 and 5 which show that the thermal energy is localized onto the low frequency modes of the acetylenic linkages. However, due to the flattened phonon dispersion curves at low frequencies (not shown for brevity), the phonon group velocities are quite small; thus, these low frequency modes cannot contribute too much to the overall heat transfer in the GNTs.

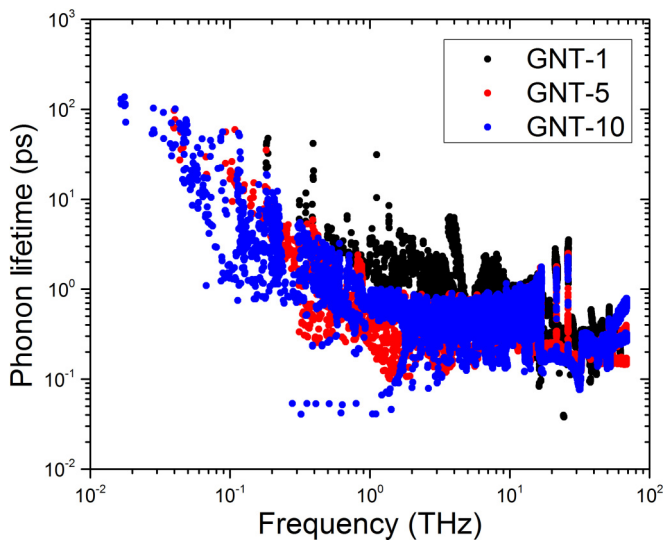


FIG. 6. (Color online) Comparison of the phonon lifetime of GNTs with different number of acetylenic linkages ( $n = 1, 5$ , and  $10$ ). All GNTs are zigzag in longitudinal direction with a diameter  $\sim 3.4$  nm.

#### IV. LENGTH AND DIAMETER DEPENDENCE OF THERMAL CONDUCTIVITY OF GNTS

It is well known that the results of the NEMD simulation might be strongly length dependent along the heat transfer direction [60,61], i.e., the axial direction of the GNTs in our simulation. Previous papers [62–64] on ordinary CNTs found that the thermal conductivity increases as the length of CNTs increases and the thermal conductivity does not converge even at a few micrometers. The length dependence of the thermal conductivity of typical GNTs (GNT-1 and GNT-10) is shown in Fig. 7(a). For GNT-1, the thermal conductivity increases largely, as the length increases from 100 to 1500 nm, while the thermal conductivity of GNT-10 has very weak length dependence over the entire length range studied here, indicating a pure diffusive phonon transport. In Fig. 7(b), we present the reciprocal of the thermal conductivity of GNTs versus the reciprocal of the length. We fitted the data points at longer lengths using a linear function [49]

$$\frac{1}{\kappa} = \frac{1}{\kappa_\infty} \left( \frac{l}{L_x} + 1 \right), \quad (6)$$

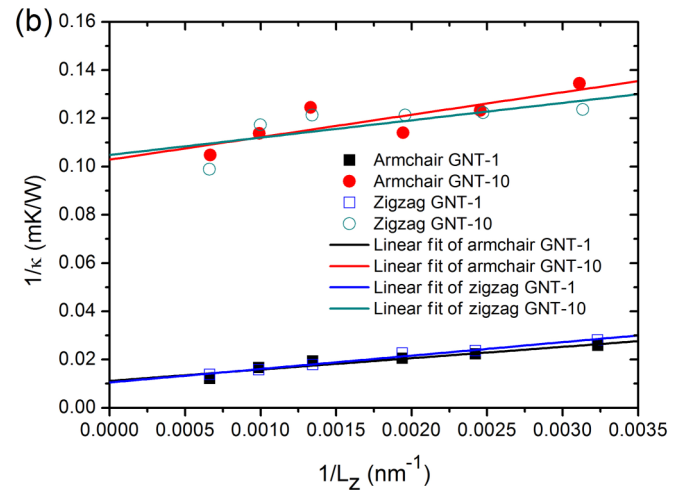
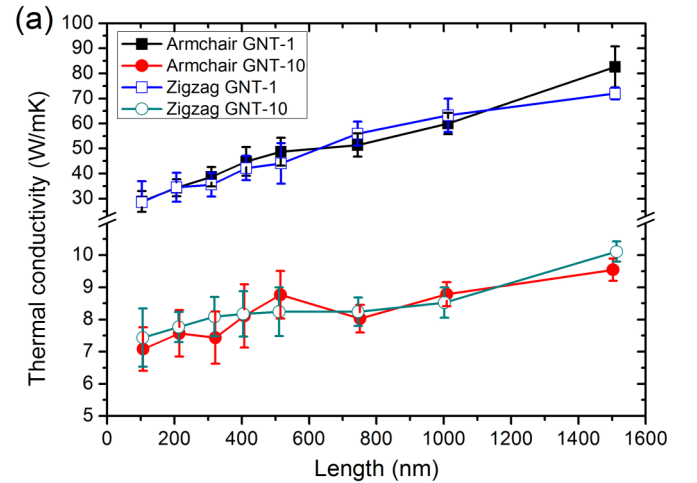


FIG. 7. (Color online) (a) Length dependence of the thermal conductivity of GNTs ( $n = 1$  and  $10$ ). Both armchair and zigzag chirality are considered. (b) The corresponding length dependence of  $1/\kappa$  on  $1/L_z$ .

where  $\kappa_\infty$  is the thermal conductivity of an infinitely long GNT and  $l$  is the effective phonon mean free path in the GNTs. The  $\kappa_\infty$  values for armchair (zigzag) GNT-1 and GNT-10 are 89.4 (94.9), 9.7 (9.5) W/mK, respectively, and the corresponding  $l$  values are 420.8 (528.2), 90.5 (68.6) nm. We have checked that after significantly increasing the simulation cells from 500 to 1500 nm, the finally converged thermal conductivity of GNT-1 and GNT-10 does not change considerably. Note that the  $l$  parameter fitted from Eq. (6) is the effective phonon mean free path and is only for qualitative comparison. The mean free paths for low frequency modes in GNTs can be longer. As evidenced by the SED calculation, the phonon mean free paths for low frequency modes can be as long as several hundred nanometers (e.g., for GNT-1, not shown for brevity), which is even longer than the effective mean free path. Nevertheless, the effective mean free path more or less indicates the relative thermal conductivity of different GNT structures, which can be seen by comparing the thermal conductivity between GNT-1 and GNT-10 and their effective mean free paths. The results in Fig. 7(a) indicate that the GNT-10 can retain the low thermal conductivity even for very long length. The phonon mean free path of GNT-10 is much shorter than that for ordinary CNTs, which is usually on the order of several hundred nanometers to a few microns. Moreover, the phonon mean free path of GNT-10 is only a few distances between the nearest hexagons, meaning that the low frequency longitudinal modes in the acetylenic linkages can only propagate a short distance along the tube, due to the weak coupling between the acetylenic linkages and hexagonal rings.

Besides the length dependence, the diameter of the GNTs could be another factor affecting the thermal conductivity. We fixed the graphyne tube length as 500 nm and varied the diameter from 0.44 to 18.3 nm. The results are shown in Fig. 8. For GNT-1, the thermal conductivity is diameter independent for a diameter larger than 2 nm. When the diameter is reduced below 2 nm, the thermal conductivity of GNT-1 steeply increases with the diameter decreasing. This trend complies with the general decrease in thermal conductivity with increasing

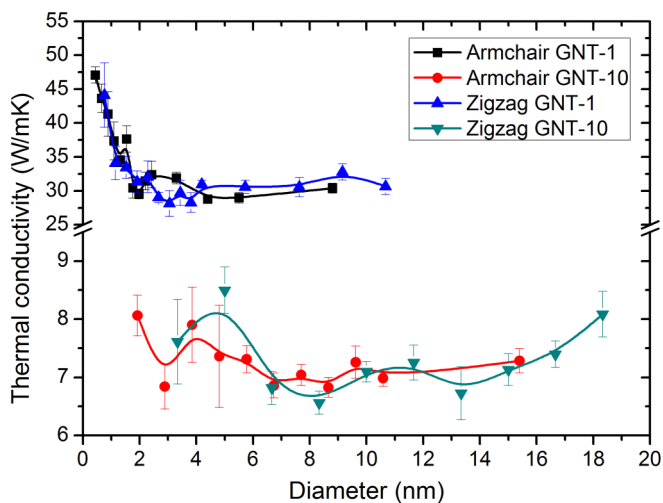


FIG. 8. (Color online) Thermal conductivity of GNTs ( $n = 1$  and 10) as a function of the nanotube diameter. All GNTs are 500 nm long. Both armchair and zigzag chirality are considered. The solid lines are guides for the eyes.

diameter for ordinary single-walled and multiwalled CNTs, which is well documented by experiments and numerical simulations [28,47]. The dependence of thermal conductivity on the CNT diameter is due to a combination of the diameter dependence of scattering rates and the change in the number of conduction channels with tube diameter. In contrast, the thermal conductivity of GNT-10 is more or less independent of diameter for the diameter ranging from 2 to 18 nm. Due to the long acetylenic linkages presented in GNT-10, it is not possible to construct a structure with an even smaller diameter. Nevertheless, the results show that the extremely low thermal conductivity (7–8 W/mK) remains for GNT-10 at all diameters, which is again dramatically lower than that for ordinary CNTs with a similar diameter. We also point out that the thermal conductivity oscillating as a function of diameter is due to the statistic error and only one finite length considered here. The error bar accounts for uncertainties both in the temperature gradient and heat flux. Since there is significant length effect in NEMD simulations, to completely compare the thermal conductivity of GNTs between different diameters, one should run all cases with different lengths and then do the same fitting as in Fig. 7 to obtain the thermal conductivity for infinite length. Since this is beyond our computational capacity, we only compare the cases for one finite length.

## V. SUMMARY AND CONCLUSIONS

In summary, we have investigated the thermal transport of GNTs by performing NEMD simulations. An unprecedentedly low lattice thermal conductivity of the GNTs (below 10 W/mK) was found among the CNTs, including the defected, doped, and chemically functionalized CNTs. The extremely low thermal conductivity stems from the unique atomic structure of the GNT, consisting of the weak acetylenic linkage ( $sp$  carbon bonds) and the strong hexagonal ring ( $sp^2$  carbon bonds). Such a structure leads to a large vibrational mismatch between these two components and thus induces significantly inefficient heat transfer along the tube. Moreover, by performing phonon polarization and SED analysis, we found that the thermal transport in the GNT is dominated by the low frequency longitudinal modes in the acetylenic linkage, especially when the number of acetylenic linkages is large ( $n \geq 6$ ). We also studied the length and diameter dependence of the thermal conductivity of GNTs. The phonon mean free path of GNT-10 is found to be as short as a few distances between the nearest hexagons, due to the weak coupling between the acetylenic linkages and hexagonal rings. We also found that the extremely low thermal conductivity of GNTs with large number of acetylenic linkages persists even for infinitely long tubes and large diameters up to  $\sim 18$  nm. Our simulation results establish a very low thermal conductivity for the special type of CNTs and indicate that thermal conductivity of CNTs can be tuned by two orders of magnitude. Our paper may offer valuable routes for design and application of GNT-related devices, such as thermoelectrics for energy conversion.

## ACKNOWLEDGMENTS

Simulations were performed with computing resources granted by the Jülich Aachen Research Alliance-High

Performance Computing (JARA-HPC) from RWTH Aachen University under Project No. jara0073. This research was supported by the National Science Foundation (NSF) of China under Grants No. 11304059 and No. 11272099, the Fundamental Research Funds for the Central Universities under Grants

No. HIT.NSRIF.2013031 and No. HIT.IBRSEM.201313, the Science and Technology Innovation Talents Special Fund of Harbin under Grant No. 2013RFQXJ003, and China Postdoctoral Science Foundation under Grant No. 2012M510938.

- 
- [1] Q. Zhang, J.-Q. Huang, W.-Z. Qian, Y.-Y. Zhang, and F. Wei, *Small* **9**, 1237 (2013).
- [2] M. F. L. De Volder, S. H. Tawfick, R. H. Baughman, and A. J. Hart, *Science* **339**, 535 (2013).
- [3] A. G. Rinzler, J. H. Hafner, P. Nikolaev, L. Lou, S. G. Kim, D. Tomanek, P. Nordlander, D. T. Colbert, and R. E. Smalley, *Science* **269**, 1550 (1995).
- [4] S. J. Tans, M. H. Devoret, H. Dai, A. Thess, R. E. Smalley, L. J. Geerligs, and C. Dekker, *Nature (London)* **386**, 474 (1997).
- [5] M. Kociak, A. Y. Kasumov, S. Gueron, B. Reulet, I. I. Khodos, Y. B. Gorbatov, V. T. Volkov, L. Vaccarini, and H. Bouchiat, *Phys. Rev. Lett.* **86**, 2416 (2001).
- [6] P. Kim, L. Shi, A. Majumdar, and P. L. McEuen, *Phys. Rev. Lett.* **87**, 215502 (2001).
- [7] T.-Y. Choi, D. Poulidakos, J. Tharian, and U. Sennhauser, *Nano Lett.* **6**, 1589 (2006).
- [8] M. M. Shulaker, G. Hills, N. Patil, H. Wei, H.-Y. Chen, H.-S. P. Wong, and S. Mitra, *Nature (London)* **501**, 526 (2013).
- [9] M. Barkelid and V. Zwiller, *Nat. Photonics* **8**, 47 (2014).
- [10] R. H. Baughman, H. Eckhardt, and M. Kertesz, *J. Chem. Phys.* **87**, 6687 (1987).
- [11] M. M. Haley, S. C. Brand, and J. J. Pak, *Angew. Chem. Int. Ed. Engl.* **36**, 836 (1997).
- [12] M. M. Haley, *Pure Appl. Chem.* **80**, 519 (2008).
- [13] F. Diederich and M. Kivala, *Adv. Mater.* **22**, 803 (2010).
- [14] G. Li, Y. Li, H. Liu, Y. Guo, Y. Li, and D. Zhu, *Chem. Commun.* **46**, 3256 (2010).
- [15] N. Narita, S. Nagai, S. Suzuki, and K. Nakao, *Phys. Rev. B* **58**, 11009 (1998).
- [16] G. Li, Y. Li, X. Qian, H. Liu, H. Lin, N. Chen, and Y. Li, *J. Phys. Chem. C* **115**, 2611 (2011).
- [17] U. H. F. Bunz, Y. Rubin, and Y. Tobe, *Chem. Soc. Rev.* **28**, 107 (1999).
- [18] V. R. Coluci, S. F. Braga, S. B. Legoas, D. S. Galvão, and R. H. Baughman, *Phys. Rev. B* **68**, 035430 (2003).
- [19] A. N. Enyashin, V. V. Ivanovskaya, Y. N. Makurin, and A. L. Ivanovskii, *Dokl. Phys. Chem.* **395**, 62 (2004).
- [20] V. R. Coluci, D. S. Galvão, and R. H. Baughman, *J. Chem. Phys.* **121**, 3228 (2004).
- [21] V. R. Coluci, S. F. Braga, S. B. Legoas, D. S. Galvão, and R. H. Baughman, *Nanotechnology* **15**, S142 (2004).
- [22] L. D. Pan, L. Z. Zhang, B. Q. Song, S. X. Du, and H. J. Gao, *Appl. Phys. Lett.* **98**, 173102 (2011).
- [23] M. Long, L. Tang, D. Wang, Y. Li, and Z. Shuai, *ACS Nano* **5**, 2593 (2011).
- [24] S. W. Cranford and M. J. Buehler, *Carbon* **49**, 4111 (2011).
- [25] Y. S. Wang, P. F. Yuan, M. Li, W. F. Jiang, Q. Sun, and Y. Jia, *J. Solid State Chem.* **197**, 323 (2013).
- [26] X.-M. Wang and S.-S. Lu, *J. Phys. Chem. C* **117**, 19740 (2013).
- [27] E. Pop, D. Mann, Q. Wang, K. Goodson, and H. Dai, *Nano Lett.* **6**, 96 (2005).
- [28] L. Lindsay, D. A. Broido, and N. Mingo, *Phys. Rev. B* **82**, 161402(R) (2010).
- [29] L. Zhu and B. Li, *Sci. Rep.* **4**, 4917 (2014).
- [30] Y. Jing, G. Wu, L. Guo, Y. Sun, and J. Shen, *Comput. Mat. Sci.* **78**, 22 (2013).
- [31] D. W. Brenner, O. A. Shenderova, J. A. Harrison, S. J. Stuart, B. Ni, and S. B. Sinnott, *J. Phys.: Condens. Matter* **14**, 783 (2002).
- [32] H. Zhong and J. R. Lukes, *Phys. Rev. B* **74**, 125403 (2006).
- [33] A. Henry and G. Chen, *Phys. Rev. Lett.* **101**, 235502 (2008).
- [34] Y. Jing, M. Hu, and L. Guo, *J. Appl. Phys.* **114**, 153518 (2013).
- [35] X. Yang, D. Chen, Z. Han, X. Ma, and A. C. To, *Int. J. Heat Mass Transf.* **70**, 803 (2014).
- [36] B. Liu, J. A. Baimova, C. D. Reddy, A. W.-K. Law, S. V. Dmitriev, H. Wu, and K. Zhou, *ACS Appl. Mater. Interfaces* **6**, 18180 (2014).
- [37] G. Barbarino, C. Melis, and L. Colombo, *Carbon* **80**, 167 (2014).
- [38] S. Plimpton, *J. Comput. Phys.* **117**, 1 (1995).
- [39] S. Nosé, *J. Chem. Phys.* **81**, 511 (1984).
- [40] W. G. Hoover, *Phys. Rev. A* **31**, 1695 (1985).
- [41] F. Müller-Plathe, *J. Chem. Phys.* **106**, 6082 (1997).
- [42] J. Che, T. Cagin, and W. A. Goddard, *Nanotechnology* **11**, 65 (2000).
- [43] C. W. Padgett and D. W. Brenner, *Nano Lett.* **4**, 1051 (2004).
- [44] R. Pan, Z. Xu, Z. Zhu, and Z. Wang, *Nanotechnology* **18**, 285704 (2007).
- [45] J. Park, M. F. P. Bifano, and V. Prakash, *J. Appl. Phys.* **113**, 034312 (2013).
- [46] D.-L. Feng, Y.-H. Feng, Y. Chen, W. Li, and X.-X. Zhang, *Chin. Phys. B* **22**, 016501 (2013).
- [47] A. M. Marconnet, M. A. Panzer, and K. E. Goodson, *Rev. Mod. Phys.* **85**, 1295 (2013).
- [48] L. Lindsay and D. A. Broido, *Phys. Rev. B* **81**, 205441 (2010).
- [49] P. K. Schelling, S. R. Phillpot, and P. Keblinski, *Phys. Rev. B* **65**, 144306 (2002).
- [50] M. Hu, K. P. Giapis, J. V. Goicochea, X. Zhang, and D. Poulidakos, *Nano Lett.* **11**, 618 (2011).
- [51] M. Hu, X. Zhang, K. P. Giapis, and D. Poulidakos, *Phys. Rev. B* **84**, 085442 (2011).
- [52] Y. Chalopin, K. Esfarjani, A. Henry, S. Volz, and G. Chen, *Phys. Rev. B* **85**, 195302 (2012).
- [53] X. Zhang, M. Hu, and D. Tang, *J. Appl. Phys.* **113**, 194307 (2013).
- [54] M. Hu, X. Zhang, and D. Poulidakos, *Phys. Rev. B* **87**, 195417 (2013).
- [55] X. Zhang, H. Xie, M. Hu, H. Bao, S. Yue, G. Qin, and G. Su, *Phys. Rev. B* **89**, 054310 (2014).
- [56] X. Zhang and J. Jiang, *J. Phys. Chem. C* **117**, 18441 (2013).
- [57] M. T. Dove, *Introduction to Lattice Dynamics* (Cambridge University Press, Cambridge, 1993).
- [58] J. M. Larkin, J. E. Turney, A. D. Massicotte, C. H. Amon, and A. J. H. McGaughey, *J. Comput. Theor. Nanosci.* **11**, 249 (2014).

- [59] J. A. Thomas, J. E. Turney, R. M. Iutzi, C. H. Amon, and A. J. H. McGaughey, *Phys. Rev. B* **81**, 081411(R) (2010).
- [60] D. P. Sellan, E. S. Landry, J. E. Turney, A. J. H. McGaughey, and C. H. Amon, *Phys. Rev. B* **81**, 214305 (2010).
- [61] C. Melis, R. Dettori, S. Vandermeulen, and L. Colombo, *Eur. Phys. J. B* **87**, 96 (2014).
- [62] G. Zhang and B. Li, *J. Chem. Phys.* **123**, 114714 (2005).
- [63] M. Alaghemandi, E. Algaer, M. C Böhm, and F. Müller-Plathe, *Nanotechnology* **20**, 115704 (2009).
- [64] B. Qiu, Y. Wang, Q. Zhao, and X. Ruan, *Appl. Phys. Lett.* **100**, 233105 (2012).